




## Direct Generation of Cartesian Grid for As-built CFD Analysis from Laser-scanned Point Clouds

Tetsuro Ishikawa<sup>1</sup> , Satoshi Kanai<sup>2</sup>  and Hiroaki Date<sup>3</sup> 

<sup>1</sup>Hokkaido University, [t\\_ishikawa@sdm.ssi.ist.hokudai.ac.jp](mailto:t_ishikawa@sdm.ssi.ist.hokudai.ac.jp)

<sup>2</sup>Hokkaido University, [kanai@ssi.ist.hokudai.ac.jp](mailto:kanai@ssi.ist.hokudai.ac.jp)

<sup>3</sup>Hokkaido University, [hdate@ssi.ist.hokudai.ac.jp](mailto:hdate@ssi.ist.hokudai.ac.jp)

Corresponding author: Satoshi Kanai, [kanai@ssi.ist.hokudai.ac.jp](mailto:kanai@ssi.ist.hokudai.ac.jp)

**Abstract.** Recently, there has been a rapid increase in the demand for as-built computational fluid dynamics (CFD) analysis, where the heat and airflow inside indoor spaces in existing buildings must be modeled and analyzed to rationalize the repair work. Accordingly, CFD grids for as-built CFD analysis must be generated to reflect the existing geometries of an indoor space to be analyzed. However, time-consuming manual operations are still required to measure the existing space, to build an accurate as-built 3D CAD model of the space, and to generate a CFD grid fitting with the CAD model. To solve this issue, this paper proposes a method to directly generate unevenly spaced Cartesian grids from laser-scanned point clouds of the existing indoor space for as-built CFD analysis. This method does not have to create any 3D CAD model in the grid generation process. It was confirmed that indoor airflow analysis could be conducted by combining the proposed method with both the simulated and real laser-scanned points. The comparison of the analysis between dense and evenly spaced grids also showed that the analysis accuracy using the unevenly spaced Cartesian grid with a smaller grid size obtained by our method was sufficiently ensured.

**Keywords:** Computational fluid dynamics, Grid generation, Laser scanning, Point clouds, Cartesian grid

**DOI:** <https://doi.org/10.14733/cadaps.2021.1341-1358>

## 1 INTRODUCTION

### 1.1 Background

Because of the growing international concern over global warming, increasing energy efficiency, and reducing energy consumption in buildings is a prime objective for energy policy at regional, national, and international levels [25]. The regulations of energy-saving efficiency in buildings have been strengthened [6], and the number of renovations of air-conditioning equipment is increasing.

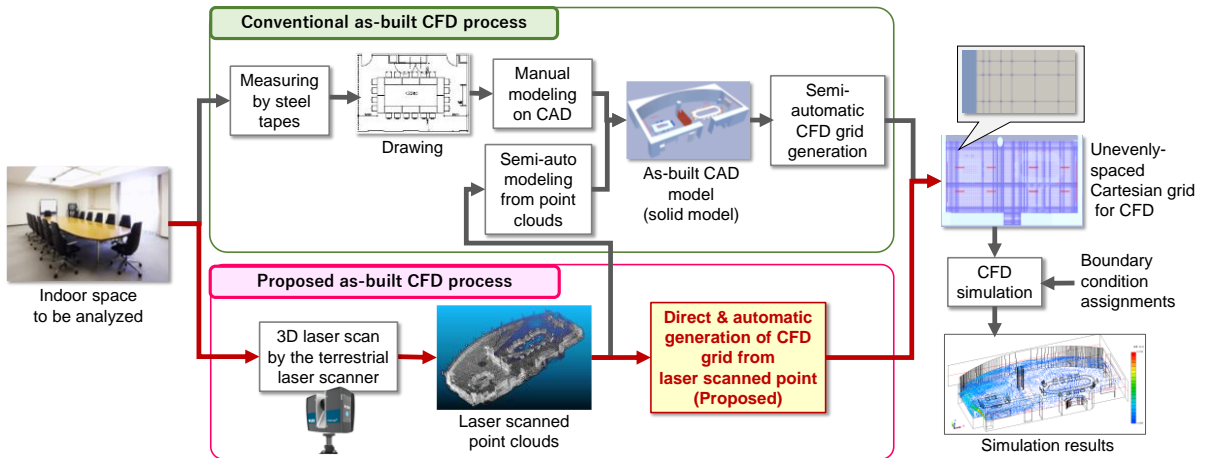


**Figure 1:** Conventional and proposed as-built CFD analysis process.

Therefore, there is also an increasing demand for as-built computational fluid dynamics (CFD) analysis, where the heat and airflow inside indoor spaces in existing buildings must be modeled and analyzed by numerical simulation to rationalize the repair work and energy retrofitting [26]. The initial and essential phase of such renovation works is to survey the heat and airflow distribution in an existing indoor living environment and evaluate the effectiveness and efficiency of existing equipment using as-built CFD analysis.

As shown in the conventional as-built CFD process of Figure 1, for the three-dimensional (3D) CFD analysis, engineers must build a 3D CAD model of the space to be analyzed, and then generate a grid for the analysis from the CAD model [7],[20],[28]. Therefore, CFD grids for as-built CFD analysis must be generated, reflecting the existing geometries of the indoor or outdoor space to be analyzed. However, because the existing indoor environment, in general, is full of a dense tangle of furniture and instruments, there is still a need for time-consuming manual operations to measure the existing space for building an accurate as-built 3D CAD model of the space and to generate a CFD grid that fits with the CAD model. Consequently, renovation design engineers currently spend enormous amounts of time and effort modeling manually as-built CAD models of such tangled environments only for CFD.

Even if a terrestrial laser scanner is introduced to improve the measurement efficiency shown in Figure 1, it is impossible to generate a complete as-built 3D CAD model of the existing spaces from the scanned point cloud fully automatically and robustly. Naturally, some commercial software to semi-automatically create CAD models from laser-scanned points exist. However, the level of their automation is imperfect, and many manual interventions remain to complete CAD models. Moreover, the small geometric features of the objects are often too simplified in CAD modeling at the engineer's discretion, and it eventually, might cause some unignorable errors in the CFD analysis.

To solve this issue, this study develops a method for automatically generating the analysis grid for as-built CFD analysis directly from laser-scanned point clouds of the existing indoor space without creating any 3D CAD model. As shown in Figure 1, in the proposed method, an unevenly spaced Cartesian grid can be generated from the point clouds because it has excellent stability of analytic calculations, the efficiency of grid point numbers, easy control of grid resolutions and geometric reproducibility of object shapes, and thus, is widely used as a grid of indoor or outdoor CFD analysis [7],[13],[15],[20],[23],[31].

However, to the authors' knowledge, only a few studies exist on automatic grid generation for as-built CFD analysis of existing indoor or outdoor spaces. Only the work of [23] was reported, where they combined terrestrial laser scanning and CFD to analyze the thermal characteristics of the outdoor space. However, they had to manually create a 3D CAD model of the town from laser-

scanned point clouds to generate the grid and did not propose any automated software to streamline the process. Of course, there is considerable research on automatic grid generation for CFD analysis [15], but they all assume that 3D watertight CAD models or triangular mesh models are given in advance for grid generation.

Unlike previous studies, as shown in Figure 1 and Figure 2, our method first performs the voxel-based spatial occupancy classification of the space using the scanned point clouds, resolves the unknown occupancy of occluded spaces, simplifies the detail geometries, estimates the object boundaries, and finally, generates the unevenly spaced Cartesian grid. The details of our proposed method are described in the following sections. We verify the validity of the method using a case study in which both simulated and real laser-scanned point clouds and commercial CFD simulation software are used with the system.

## 1.2 Functional Requirements and Our Approaches

The requirements from the aspect of grid generation for as-built CFD analysis of indoor spaces from laser-scanned point clouds are summarized below.

- (1) The object surface and space should be correctly distinguished and gridded, based only on the scanned point clouds.
- (2) The spatial occupancy of occluded space caused by laser scanning should be estimated plausibly.
- (3) Some special objects (heat source, louver, etc.) to which the boundary conditions of the analysis are added should be automatically detected in the point clouds.

Furthermore, the requirements from the aspect of the unevenly spaced Cartesian grid generation are listed below.

- (4) The adjacent grid width must be monotonically increased with the distance from object surfaces, and the ratio must be less than the maximally allowable ratio  $r$  (usually less than 2.0).
- (5) The aspect ratio of three grid-widths along the orthogonal axes must be less than the threshold aspect ratio  $q$  (usually less than 10).
- (6) To speed up the calculations and improve the stability of CFD simulation, the geometry of the fine details of the object surface should be simplified or omitted optionally in grid generation from a practical viewpoint when they are not expected to significantly affect the mainstream of the airflow.

Among them, we realized the requirements of (1), (2), (4), and (6) in this study, and the implementation of (3) and (5) remain as future studies.

For these requirements to be realized, voxel representation is critical in the processing pipeline of our developed system. To realize requirement (1), we first decompose the analysis space into voxels, and their spatial occupancies (*free/occupied/unknown*) are directly determined from the locations of the scanners and scanned points. For realizing requirement (2), the system automatically visualizes the occluded spaces as clusters of unknown voxels, and the user can interactively assign the estimated occupancy (*free/occupied*) to each voxel cluster. Furthermore, to realize requirement (4), the grid-width ratio can be automatically and easily adjusted to increase with distance from the surfaces of *occupied* voxels, while keeping the threshold-common ratio of the grid-width. Finally, to realize requirement (6), we apply a simple morphology-like transformation to the cluster of the *occupied* voxels to suppress the fine detail geometries unnecessary for grid generation and analysis.

The latter part of the paper is organized as follows. Section 2 introduces the related work and discusses its applicability. The technical details of the grid generation pipeline in our system are described in detail in Section 3. Section 4 validates the effectivity of the grid generation system using some case studies, and Section 5 summarizes the conclusions and future studies.

## 2 RELATED WORK

### 2.1 Reconstruction of Building Indoor Models from Laser Scanning

The development of indoor scanning and point cloud generation methods sparked a growing demand for 3D models of building indoor space in many applications in construction, indoor navigation, and real estate management [19]. Currently, laser scanners are widely used to capture massive point clouds for building indoor surfaces quickly and highly detailed [19]. However, the conversion process from point clouds to building indoor models remains largely a time-consuming and error-prone manual process [22].

To solve this problem, many papers have reported about the automatic reconstruction methods of 3D building indoor models represented by CAD-grade solid models from laser-scanned point clouds [17],[22],[24],[32],[34]. In general, their reconstruction methods consist of segmentation of the point clouds into the sub-clouds with semantic class labels such as walls, ceilings, and floors, and fitting the parametric model to the sub-clouds. The review of [29] summarizes the related techniques of the automatic reconstruction of building information models from laser-scanned point clouds. Commercial software has also been available for converting point clouds to CAD-grade models of pipework and structures [14].

The automatic reconstruction of building indoor models was somewhat realized so far. However, unfortunately, fully automatic and complete reconstruction of indoor models from laser-scanned points have yet to be realized because of the measurement errors, non-uniform sampling density, and occlusions of the scanned data. Therefore, it is impossible to generate a complete CAD-grade solid model of the existing spaces from the scanned point cloud fully automatically and robustly. Conversely, direct grid generation from the laser-scanned point clouds without creating any CAD-grade solid model of indoor space is beneficial to streamline the as-built CFD process and to reduce errors in grid generation.

### 2.2 Application of Laser Scanning to Structural Analysis

Several applications of laser scanning to the structural analysis using the finite element method (FEM) were recently reported in the area of historical building conservation. In [4], they developed a semi-automatic procedure to transform laser-scanned point clouds of a historical building into 3D finite element models. Their procedure starts from capturing point clouds scanned from inside and outside the building, and the clouds are converted to a set of slices, each of which contains two-dimensional (2D) points. In each slice, the slice is first cleaned to eliminate the noisy points, the internal and external polygons are fitted to the points, and the polygons are then described by a binary image with a specific resolution to generate the 3D voxel element model for FEM. They performed the bending mode analysis and compared their results with the FEM obtained from a CAD-grade solid model. [5] applied a similar method to linear and nonlinear pushover analysis and the crack pattern analysis. However, in both studies, manual interventions were still required for the latter part of their procedure, including slice cleaning and splitting the internal/external points. They also do not discuss how to ignore or approximate the detailed geometry of the object surface unnecessary for analysis and how to estimate the spaces unmeasured in laser scanning plausibly.

Another voxelization-based method similar to [4-5] also transformed point clouds from aerial and terrestrial laser scanning of a building façade into solid models for their structural analysis using FEM [11]. The transformation procedures are fully automated, but they only applied their method to simply-shaped façade structures, and the issues similar to the above are not discussed well.

The application of laser scanning to the safety analysis of cultural heritages [10], bridges [21], and historic buildings [2] are also conducted, where laser-scanned point clouds are used to create the FEM model. However, their transformation procedures must first create solid models of the building from laser-scanned point clouds, and then, FE models are automatically generated from the solid models. However, as stated above, it is practically challenging to create CAD-grade solid models

from the point clouds fully automatically; therefore, time-consuming manual interventions are still needed for the modeling and grid generation, even by combining commercial software.

### 2.3 Application of Laser Scanning to CFD

As the heat-island phenomenon, created by heat emissions in the metropolitan area, is exacerbating environmental problems in urban areas, city-scale CFD simulation is frequently used to predict the phenomenon and assess the urban microclimate. The town-scale CFD analysis is applied, for example, to the pedestrian wind comfort around buildings [16] and the heat rejection from air-conditioners [13]. The complete review of CFD analysis of the urban microclimate is presented in [31]. To conduct the CFD simulation, a grid generation is needed. However, in most simulations, the building geometry for grid generation is manually created by referring to town maps, orthophotos, or polygon data in geographic information systems (GIS). In some cases, 3D city models are used for the automatic CFD grid generation [3].

CFD simulation has been proactively applied to predict heat and airflow in indoor built environments. The simulation analyzes building energy performances [7], predicts natural ventilation performance [28], and estimates local air movement for personalized ventilation [20].

However, unlike the applications to the structural analysis, laser scanning has not yet been effectively used in CFD grid generation and simulation. To the authors' knowledge, only the work of [23] proposes the as-built CFD simulation, where they created a town-wide CFD grid for the urban thermal environment analysis from point clouds captured by a terrestrial laser scanner. However, in their approach, a CAD-grade solid model of the town must be created from the scanned point clouds using manual operations to generate the CFD grid. Unfortunately, the authors of [23] do not propose any automated solution to automated grid generation from the laser-scanned point clouds.

Overall, there are few studies on automatic grid generation for as-built CFD analysis of existing indoor spaces from laser-scanned point clouds.

## 3 AS-BUILT CFD GRID GENERATION ALGORITHM FROM LASER-SCANNED POINT CLOUDS

Figure 2 shows the processing pipeline of our grid generation method from laser-scanned point clouds. The pipeline accepts a set of laser-scanned point clouds, where a closed indoor space is measured from different scanner locations. It finally outputs the unevenly spaced Cartesian grid information for as-built CFD analysis, where each grid point inside the object is labeled as *object*, and the other grid points are labeled as *space*. We confirmed that this Cartesian grid could be imported by some commercial CFD software. In CFD software, the boundary conditions

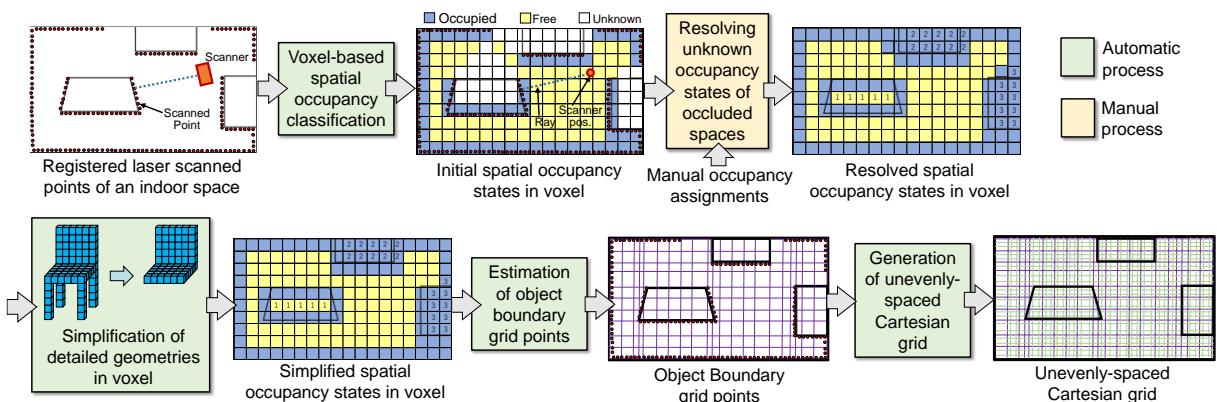


**Figure 2:** Processing pipeline of the proposed grid generation method from laser-scanned point clouds.

corresponding to the heat sources and air inlets/outlets are manually assigned to the subsets of the grid points in CFD software to conduct the simulation.

In the processing of grid generation from laser-scanned point clouds, we assume that all the point clouds have already registered each other, the dominant axes of the indoor space boundaries such as the walls and ceilings are already aligned to the orthogonal axes of the Cartesian grid, and the scanned point resolution is much denser than the Cartesian grid width. In the processing pipeline of Figure 2, the spatial occupancy classification, simplification of detailed geometries, and estimation of object boundary grid points are performed fully automatically, while the process of resolving unknown occupancy states of occluded spaces must be done manually. The processing details are described in the following subsections.

### 3.1 Voxel-based Spatial Occupancy Classification

First, the indoor space to be analyzed is partitioned into voxels, and the spatial occupancy of each voxel is classified by performing ray-casting between a voxel and the line connecting a scanned point with the scanner position. As shown in Figure 2, the spatial occupancy is classified into three states, namely occupied, free, and unknown, which are similar to [33]. Occupied means that the voxel includes at least one scanned point and a piece of an object surface exists in the voxel. Alternatively, free means that the ray from a scanner position to a scanned point passes through the voxel and the voxel exhibits a free space. Moreover, unknown means that the spatial occupancy of the voxel cannot be determined uniquely.

In the process, the occupancy state of all voxels is initialized as unknown. Then, the voxels with any scanned point are set as occupied, and those intersected with the ray are set as free. Our modified version of OctoMap [12], which is a software library of 3D occupancy grid mapping, performed the occupancy classification process.

### 3.2 Resolving Unknown Occupancy States of Occluded Spaces

In laser scanning, the unknown voxel always remains where any scanned point cannot be acquired because of the occlusion. However, the unknown voxel is not allowed for generating the CFD grid, and unfortunately, the system cannot classify the real occupancy state of the unknown voxel uniquely and automatically. Therefore, the user must interactively assign the free or occupied label to these unknown voxels to solve the uncertainty of the occupancy.

Because the number of the unknown voxels is large, it is inefficient to ask the user to assign a free or occupied label to the voxels one-by-one. Instead, first, the connected unknown voxels are automatically pre-clustered using a 3D labeling algorithm. Then, the clusters are graphically shown to the user, and the user is prompted to interactively assign the free or occupied label to each cluster. Even if there is a large number of unknown voxels, the number of clusters is much less than the voxels themselves because these voxels tend to be crowded locally. Therefore, this manual label assignment operation is not significantly time-consuming. This user interaction for the label assignment is performed with visualization software (ParaView [1]).

### 3.3 Simplification of Detail Geometries

In CFD analysis, from the efficiency and stability aspect of the simulation, the geometries of small and thin parts, such as chair legs, were often simplified or omitted in the grid generation when they are not expected to have a significant effect on the mainstream of the airflow. Therefore, the occupied voxel representing the small and thin shape is changed to the free voxel by using the following 3D morphology-like operations.

First, the voxel space is scanned with the  $N \times N \times 1$  structuring element, as shown in Figure 3(a). If one or more occupied voxels exist in the element, the voxel of interest is labeled as occupied (Figure 3(c)). Then, the space is scanned again with the same element, and if one or more free voxels exist, the voxel of interest is labeled as free (Figure 3(d)). Then, these operations are



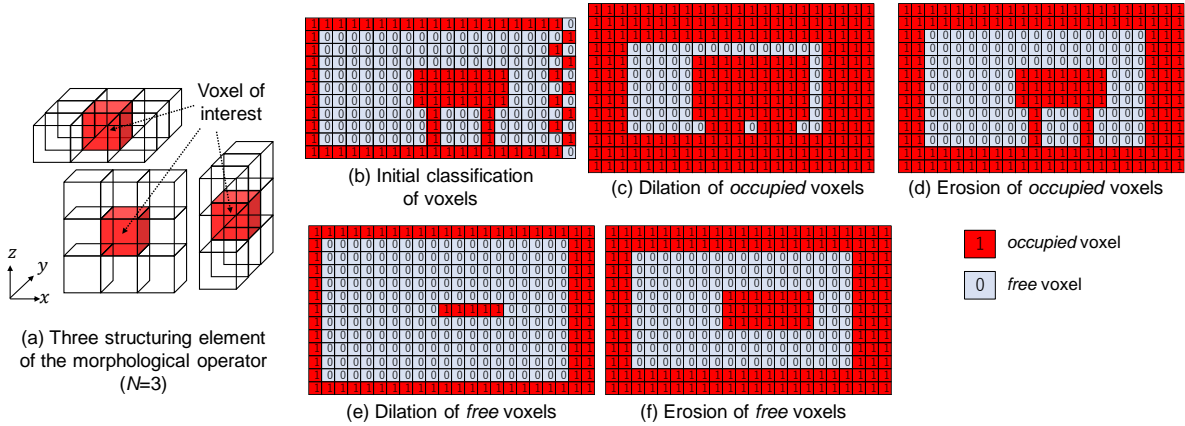


**Figure 3:** Simplification of detail geometries by morphological operators.

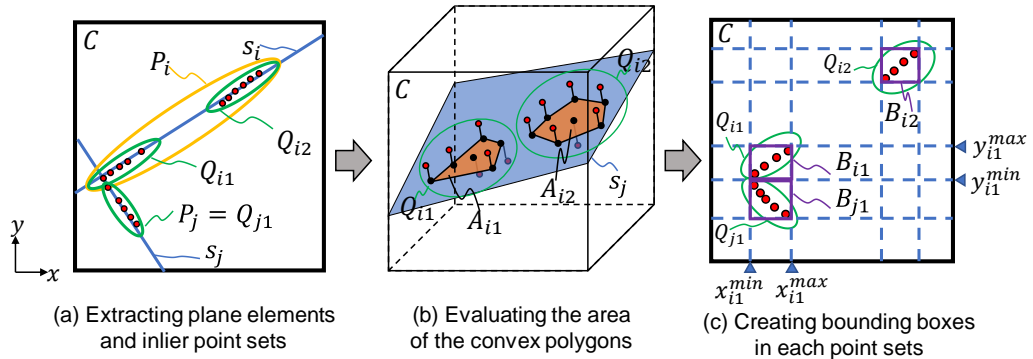


**Figure 4:** Estimation of object boundary grid points.

repeated (Figure 3(e)(f)). Finally, these operations are performed independently for three different structuring elements along the  $x$ -,  $y$ -, and  $z$ -axes, and the voxels that represent free for all the structuring elements is finally labeled as free.

Because of the operation, thin columnar clusters of occupied voxels, with two of the three thicknesses along the orthogonal axes smaller than the  $N$  voxels, are removed, and their occupancy label is switched to free.

If cross-flow objects are expected to exert a significant influence on the mainstream, they should not be simplified or omitted. Moreover, if we have laser-scanned point clouds and the analysis scale is not so large, the simplification of detailed geometries is dispensable. Therefore, this simplification process should be optionally performed.

### 3.4 Estimation of Object Boundary Grid Points

The detailed position of the object boundary surface existing in an occupied voxel is then estimated, as shown in Figure 4. First, as shown in Figure 4(a), we estimate the least-square plane elements  $s_i (\in S_c)$  that fit the scanned points in a voxel  $C$  by plane-type RANSAC, where  $s_i$  is a plane element and  $S_c$  is a set of all plane elements included in  $C$ . If RANSAC finds multiple plane elements in  $C$ , then all elements are stored in  $S_c$ . Then, we extract the inlier point set  $P_i$  of a plane element  $s_i$  from the point clouds included in  $C$  and perform the Euclidian clustering of  $P_i$  to partition  $P_i$  into the sub-point sets  $Q_{i1}, Q_{i2}, \dots$ .

Next, as shown in Figure 4(b), we project the sub-point set  $Q_{ij}$  onto the plane element  $s_i$  and evaluate the area of the convex polygon  $A_{ij}$  of the projected sub-point set  $Q_{ij}$ . If  $A_{ij}$  is greater than or equal to a threshold  $\tau_{ij}$ , we generate an axis-aligned-bounding-box  $B_{ij}$  that encloses  $Q_{ij}$ .

Finally, as shown in Figure 4(c), we insert the maximum and minimum coordinates  $(x_{ij}^{min}, x_{ij}^{max})$ ,  $(y_{ij}^{min}, y_{ij}^{max})$ , and  $(z_{ij}^{min}, z_{ij}^{max})$  of  $B_{ij}$  into the elements of the boundary sequences  $X_L, Y_L, Z_L$ , each of which is a one-dimensional sequence of real numbers. The coordinates  $(x_l, y_m, z_n) \in X_L \times Y_L \times Z_L$  finally constitutes each grid point on the object boundaries. When an interval between two consecutive elements in the sequence is smaller than the threshold, it is integrated into one element.

### 3.5 Generation of Unevenly Spaced Cartesian Grid

Based on the estimated grid points of the object boundaries, the coordinates of unevenly spaced Cartesian grids included in a free voxel are independently calculated along the  $x, y$ , and  $z$ -directions, and are inserted between two consecutive elements originally stored in the boundary sequences  $X_L, Y_L, Z_L$ .

Because the fluid flow velocity changes significantly as it approaches the object boundary, a finer grid is needed near the boundary. Therefore, the width of unevenly spaced Cartesian grids to be inserted should increase with the increasing distance from the boundary. Reflecting this, the coordinates of unevenly spaced Cartesian grids are calculated as discussed below.

Given that a boundary sequence  $X_L$  is defined as  $X_L = \langle x_0, x_1, x_2, \dots, x_l, x_{l+1}, \dots \rangle$ , we want to generate a set of new  $x$ -coordinates of unevenly spaced Cartesian grids and insert them between an interval  $[x_l, x_{l+1}]$  under the conditions that  $d_{max}$  and  $d_{min}$  are given as the maximum and minimum target grid width, and  $r$  is given as the maximum allowable ratio between an adjacent grid width. We must determine a monotonically-increasing sequence of the coordinates of the newly inserted grids  $U = \langle u_0 (= x_l), u_1, u_2, \dots, u_n, \dots, u_{n_{max}-1}, u_{n_{max}} (= x_{l+1}) \rangle$  between  $x_l$  and  $x_{l+1}$ .

To determine the sequence  $U$ , as shown in Figure 5, we consider that an adjacent grid width  $d_n = u_n - u_{n-1}$  should increase in distance from  $u_0 (= x_l)$  or  $u_{n_{max}} (= x_{l+1})$  according to the geometric progressions  $d_n = d_{min} \cdot r^{n-1}$  with the first term  $d_{min}$  and the common ratio  $r$ . We also assume that the grid width should remain  $d_{max}$  if  $d_n \geq d_{max}$ .

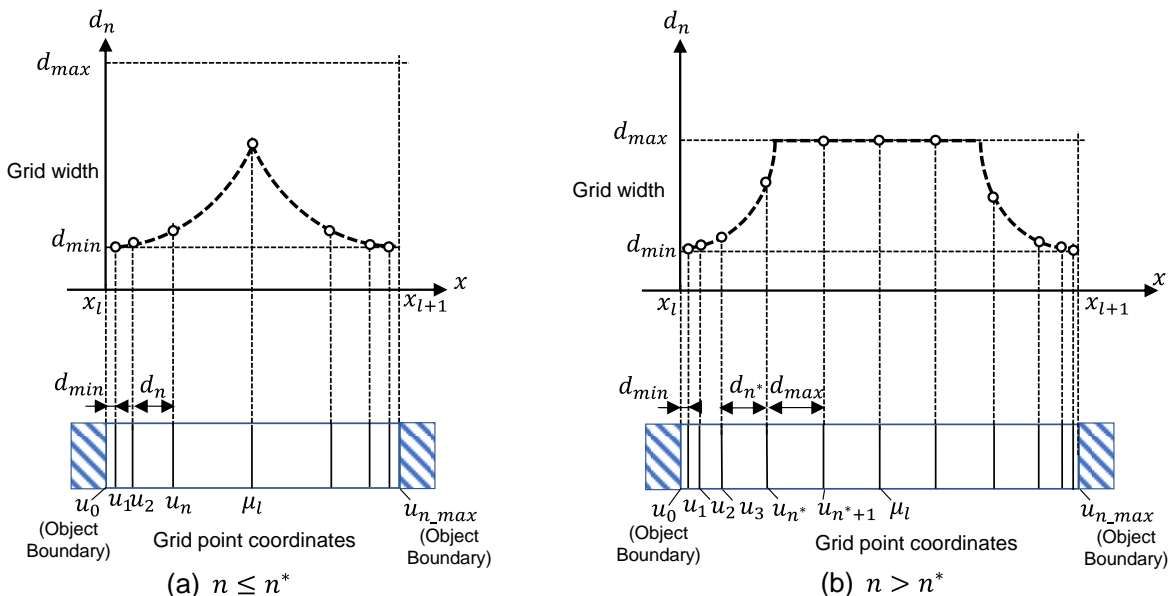


Figure 5: Generation of the grid point coordinates of the unevenly spaced grid.



Based on that consideration, the coordinates of the newly inserted grids  $u_1, u_2, \dots, u_n, \dots, u_{n_{max}-1}$  of the sequence  $U$  are determined by the following procedure:

- 1) Initialize  $U$  as  $U \leftarrow \langle u_0(= x_l), u_{n_{max}}(= x_{l+1}) \rangle$ .
- 2) Evaluate an integer  $n^*$  indicating how many grid points are allowed from the grid width  $d_{min}$  to  $d_{max}$  by using Equation (3.1):

$$n^* = \left\lceil \log_r \frac{d_{max}}{d_{min}} + 1 \right\rceil \quad (3.1)$$

- 3) Evaluate the midpoint coordinate between  $x_l$  and  $x_{l+1}$  as  $\mu_l = \frac{1}{2}(x_l + x_{l+1})$ , and find an integer  $n_\mu$  by Equations (3.4) and (3.5) such that Equations (3.2) and (3.3) hold:

$$x_l + \frac{d_{min}(r^{n_\mu-1} - 1)}{r - 1} \leq \mu_l \leq x_l + \frac{d_{min}(r^{n_\mu} - 1)}{r - 1} \quad (3.2)$$

$$x_{l+1} - \frac{d_{min}(r^{n_\mu} - 1)}{r - 1} \leq \mu_l \leq x_{l+1} - \frac{d_{min}(r^{n_\mu-1} - 1)}{r - 1} \quad (3.3)$$

$$n_\mu = \begin{cases} \left\lceil \log_r \frac{(\mu_l - x_l)(r - 1)}{d_{min}} + 1 \right\rceil & (\mu_l \leq u_{n^*}) \\ \left\lceil \frac{\mu_l - u_{n^*}}{d_{max}} + n^* \right\rceil & (\mu_l > u_{n^*}) \end{cases} \quad (3.4)$$

$$u_{n^*} = x_l + \frac{d_{min}(r^{n^*} - 1)}{r - 1} \quad (3.5)$$

where  $n_\mu - 1$  indicates how many grid points can be included between  $u_0(= x_l)$  and  $\mu_l$  or between  $\mu_l$  and  $u_{n_{max}}(= x_{l+1})$ .

- 4) Generate a sequence of the ascending coordinates  $U^+ = \langle u_1^+, u_2^+, u_3^+, \dots, u_{n_\mu-1}^+, u_{n_\mu}^+ \rangle$  by using Equation (3.6), and append  $U^+$  to  $U$ :

$$u_n^+ = \begin{cases} x_l + \frac{d_{min}(r^n - 1)}{r - 1} & (n \leq n^*) \\ u_{n^*}^+ + d_{max}(n - n^*) & (n > n^*) \end{cases} \quad (n = 1, 2, \dots, n_\mu - 1, n_\mu) \quad (3.6)$$

- 5) Generate a sequence of the ascending coordinates  $U^- = \langle u_{n_\mu}^-, u_{n_\mu-1}^-, \dots, u_2^-, u_1^- \rangle$  by using Equation (3.7), and append  $U^-$  to  $U$ :

$$u_n^- = \begin{cases} x_{l+1} - \frac{d_{min}(r^n - 1)}{r - 1} & (n \leq n^*) \\ u_{n^*}^- - d_{max}(n - n^*) & (n > n^*) \end{cases} \quad (n = 1, 2, \dots, n_\mu - 1, n_\mu) \quad (3.7)$$

- 6) Generate the coordinate of the additional grid point  $u_a^+$  between  $u_{n_\mu-1}^+$  and  $u_{n_\mu}^+$  in  $U^+$  defined by Equation (3.8), and insert  $u_a^+$  into  $U$ :

$$u_a^+ = \begin{cases} \frac{u_{n_\mu}^+ - \mu_l}{2} & (|\mu_l - u_{n_\mu-1}^+| \leq |u_{n_\mu}^+ - \mu_l|) \\ \frac{\mu_l - u_{n_\mu-1}^+}{2} & (|\mu_l - u_{n_\mu-1}^+| > |u_{n_\mu}^+ - \mu_l|) \end{cases} \quad (3.8)$$

- 7) Similar to 6), generate the coordinate of the additional grid point  $u_a^-$  between  $u_{n_\mu}^-$  and  $u_{n_\mu-1}^-$  in  $U^-$  defined by Equation (3.9), and insert  $u_a^-$  into  $U$ :

$$u_a^- = \begin{cases} \frac{\mu_l - u_{n_\mu}^-}{2} & (|\mu_l - u_{n_\mu}^-| \geq |u_{n_\mu-1}^- - \mu_l|) \\ \frac{u_{n_\mu-1}^- - \mu_l}{2} & (|\mu_l - u_{n_\mu}^-| < |u_{n_\mu-1}^- - \mu_l|) \end{cases} \quad (3.9)$$

- 8) Insert  $\mu_l$  into  $U$ , and remove  $u_{n_\mu-1}^+$ ,  $u_{n_\mu}^+$ ,  $u_{n_\mu}^-$ , and  $u_{n_\mu-1}^-$  from  $U$ .

This grid generation is also independently applied to the y and z-directions to complete the unevenly spaced Cartesian grids.

Finally, for all generated grid points, including the unevenly-spaced Cartesian grids, if a grid point  $g_{ijk} = (x_i, y_j, z_k)$  exists inside an occupied voxel or exists at any object boundary, i.e.,  $(x_i \in X_L) \wedge (y_j \in Y_L) \wedge (z_k \in Z_L)$ , the object/space attribute  $f$  of this grid point is labeled as object as  $f(g_{ijk}) = object$ , otherwise the point is labeled as space as  $f(g_{ijk}) = space$ . This object/space attribute  $f$  assigned to a grid point is finally used in CFD simulation software.

#### 4 CASE STUDIES OF GRID GENERATION AND CFD ANALYSIS

##### 4.1 Grid Generation from Simulated Laser Scanned Point Clouds

As a preliminary case study, we performed laser scan simulation by using the robot sensor simulation software BlenSor [9] on the 3D CAD model of an indoor space, as shown in Figure 6 (a meeting room, including furniture with a width of 17.5 m, depth of 9.0 m, and height of 2.6 m), and generated the simulated point clouds. The scanner model was placed at eight different locations in the room, as shown in Figure 6(a), and eight different scanned point clouds of about 540,000 points/scans were obtained, as shown in Figure 6(b). Because these simulated point clouds were generated under one global coordinate system in the robot sensor simulation software, we did not need the registration among the point clouds.

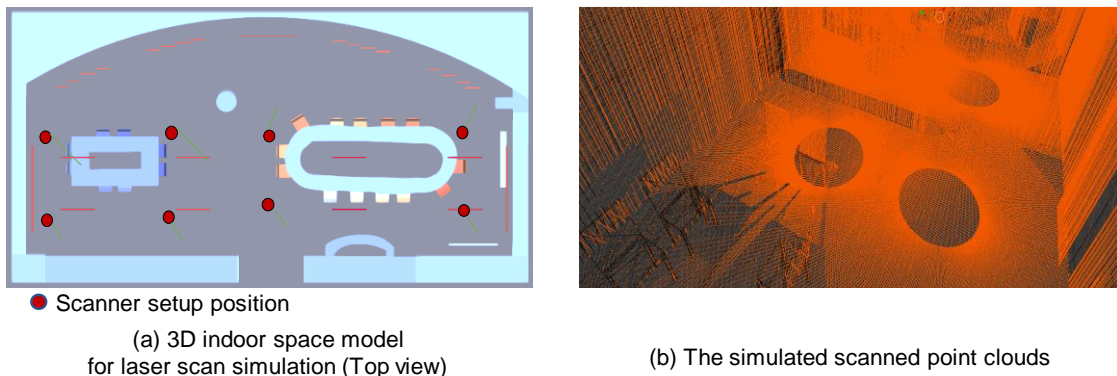


**Figure 6:** Indoor space model and simulated scanned point clouds.

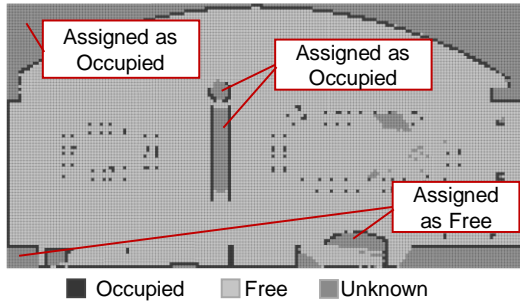


**Figure 7:** Spatial occupancy classification results and the interactive occupancy assignments to the unknown voxel clusters.

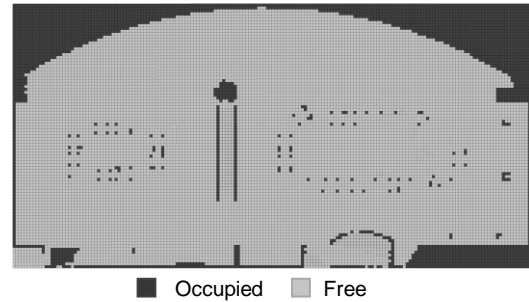


**Figure 8:** Spatial occupancy classification results after resolving the unknown occupancy states.

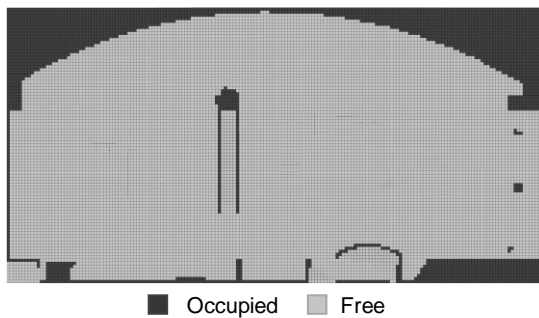


**Figure 9:** Spatial occupancy classification after simplifying the detail geometries.

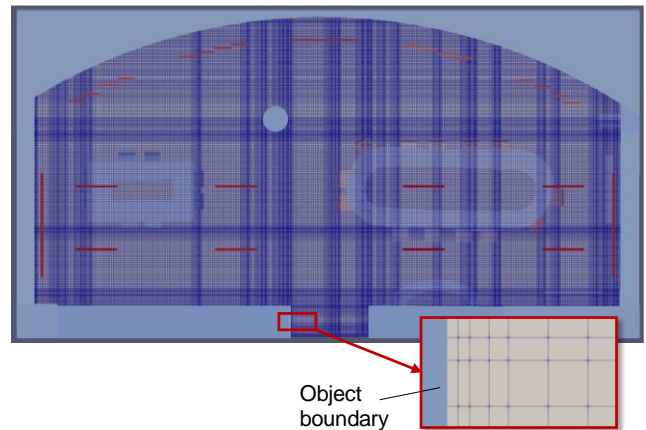


**Figure 10:** Unevenly spaced Cartesian grid automatically generated from the voxel of Figure 9.

Figure 7 shows the spatial occupancy near the floor generated from the point clouds when the voxel resolution is 0.1 m. After interactively assigning the occupancy state of a few unknown voxel clusters caused by the occlusions, as indicated in Figure 7, we can determine the occupancy states of these clusters, as shown in Figure 8. This interactive assignment took approximately 10 minutes.

Then, from the analysis engineer's suggestion, the small geometries of the furniture, such as chair legs, did not have a significant effect on the mainstream of the air in this room. Therefore, the detailed geometry was automatically simplified, and the final occupancy state was obtained, as shown in Figure 9. As shown in Figure 9, the unnecessary details for analysis, such as the chair legs, were deleted in the voxel space.

Finally, as shown in Figure 10, the unevenly spaced Cartesian grid was automatically generated from the voxel in Figure 9. The parameters of grid generation were specified as  $d_{max} = 0.1$  m,  $d_{min} = 0.025$  m, and  $r = 2$ ,  $\tau_{ij} = (\text{area of an equilateral triangle with a side of } 5\sqrt{2} \text{ cm})$ . The number of grid points in each orthogonal axis was 559 points in width, 355 in depth, and 98 in height. The grid generation time was 6 min 46 sec on a personal computer (CPU: Corei7-5960X), excluding the user interaction time. The maximum and minimum grid widths in each axis were 0.131 and 0.025 m in the x-axis, 0.1 and 0.025 m in the y-axis, and 0.1 and 0.025 m in the z-axis.

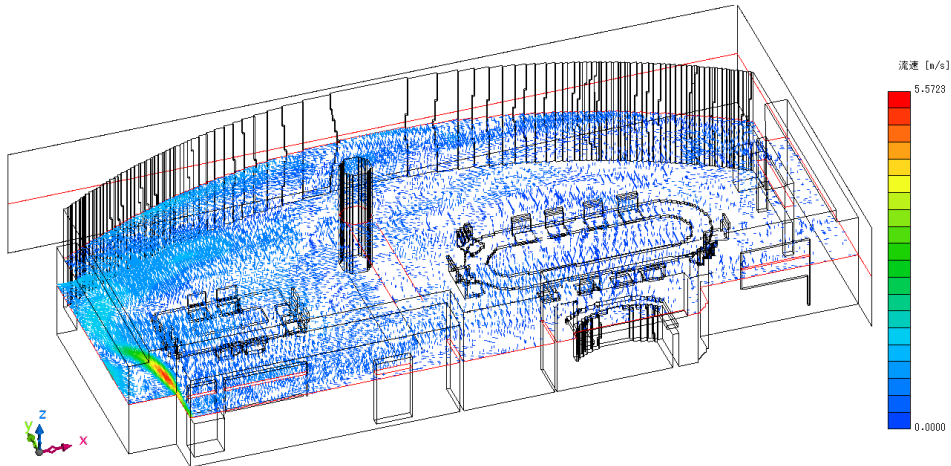


**Figure 11:** Airflow simulation result at a specified height using the Cartesian grid of Figure 10.

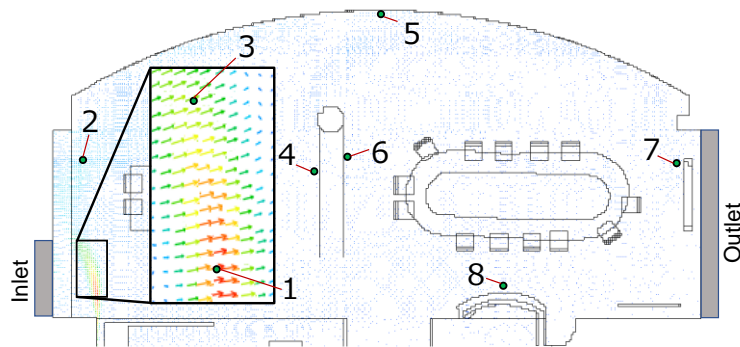


**Figure 12:** Eight sampled grid points for flow velocity verification.

| Location           | Flow velocity [m/s]      |                         | Absolute difference [m/s]<br>( $C =  A - B $ ) | Percentage [%]<br>( $100 \times C/B$ ) |
|--------------------|--------------------------|-------------------------|--|--|
|                    | Unevenly spaced grid (A) | Equally spaced grid (B) |  |  |
| 1                  | 5.6067                   | 5.5723                  | 0.0344   | 0.6173                                 |
| 2                  | 0.2787                   | 0.2786                  | 0.0001   | 0.0359                                 |
| 3                  | 3.0392                   | 3.0646                  | 0.0254   | 0.8288                                 |
| 4                  | 0.2257                   | 0.2245                  | 0.0012   | 0.5345                                 |
| 5                  | 0.1646                   | 0.1653                  | 0.0007   | 0.4235                                 |
| 6                  | 0.0024                   | 0.0024                  | 0.0000   | 0.0000                                 |
| 7                  | 0.2000                   | 0.2003                  | 0.0003   | 0.1498                                 |
| 8                  | 0.2209                   | 0.2214                  | 0.0005   | 0.2258                                 |
| Average difference |                          |                         | 0.0078   |  |

**Table 1:** Difference in flow velocities at sampled points.

#### 4.2 CFD Simulation using the Automatically Generated Cartesian Grid

A simple airflow velocity analysis of the air conditioning system was performed with CFD simulation software (scSTREAM [27]) using the unevenly spaced grid, generated from the simulated scanned points above. Since the object/space attribute was already assigned for each grid point in the grid

imported to the simulation software, the grid was directly used for the simulation, except for the boundary condition assignments, and no decimation of the grids was performed. After importing the grid, we manually assigned the boundary conditions to subsets of the grid points in the simulation software so that the air inlet was placed on the bottom of the left wall and the outlet was on the entire right wall. Figure 11 shows the analysis result. The velocity peak appeared near the inlet. The CFD simulation took 5 h 32 min for predicting the phenomenon for 33 sec.

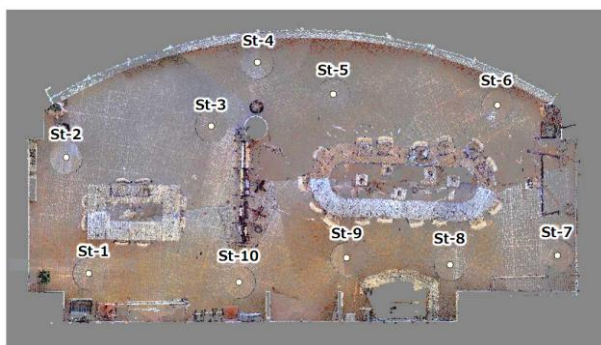
To confirm the results above, a similar flow analysis using a dense equally spaced Cartesian grid was performed for comparison. The grid width was 0.025 m, which was the same as the minimum grid width of the automatically generated unevenly spaced grid, generated from the simulated laser-scanned point. The number of grid points was 700 in the width, 360 in the depth and 104 points in the height. The analysis time was 6 h 03 min under the same conditions.

Table 1 shows the difference in the flow velocity between the unevenly spaced grid and equally spaced one at eight sampled grid points, as shown in Figure 12. As summarized in Table 1, the absolute difference in flow velocity between the equally spaced and unevenly spaced grids was less than 1% of the velocity in the evenly spaced grid. The unevenly spaced grid generated from the laser scan using our method can, therefore, be used for CFD analysis in the same manner as the dense equally spaced grid. The total number of the unevenly spaced grid points reduced to 75% of that of the dense equally spaced grid.

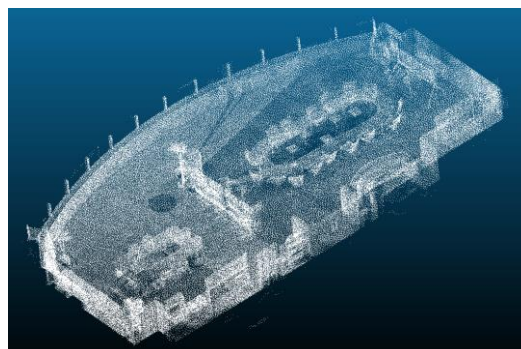
### 4.3 Grid Generation and CFD Analysis from Real Laser-Scanned Point Clouds

As a final case study, real point clouds are captured from a meeting room similar to Section 4.1 using a terrestrial laser scanner (Z+F IMAGER 5010C). The scanner was placed at ten different locations in the room, as shown in Figure 13(a), and ten different scanned point clouds of about 2 million points/scans and, in total, 19 million points were obtained, as shown in Figure 13(b).

In the case study, registration among the point clouds were necessary as a preprocessing for the grid generation. Therefore, we used a marker-less registration function in a commercial point cloud processing software. Because the number of point clouds and scans were small (10 scans), the registration could be performed fully automatically in the commercial software. The whole registration took approximately 15 minutes. It was comparable in time to the grid generation in our system, and the registration time was not necessarily considered as the rate-determining step. Figure 14 shows the spatial occupancy near the floor generated from the point clouds when the voxel resolution is 0.1 m. After interactively assigning the occupancy state of around 20 unknown voxel clusters, the occupancy states of these clusters can be determined, as shown in Figure 15. This



(a) Laser scanned point clouds of an indoor space and the scanner setting locations (Top view)



(b) Ten scanned point clouds after registered

**Figure 13:** Real scanned point clouds of an indoor space captured by a terrestrial laser scanner.





**Figure 14:** Spatial occupancy classification results before interactive occupancy assignments to the unknown voxel clusters.



**Figure 15:** Spatial occupancy classification results after resolving the unknown occupancy states.



**Figure 16:** Spatial occupancy classification after simplifying the detail geometries.

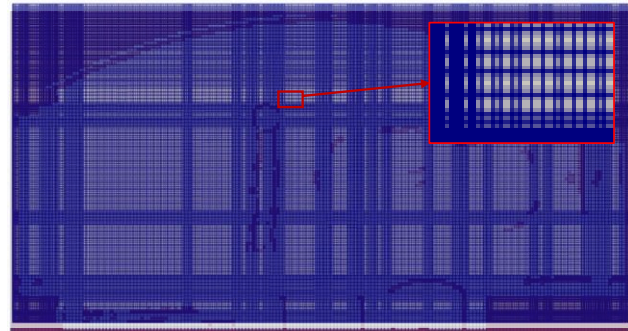


**Figure 17:** Unevenly spaced Cartesian grid automatically generated from the voxel of Figure 16.

interactive assignment work took approximately 15 minutes. Then, we simplified the detailed, and obtained the final occupancy state, as shown in Figure 16. Here, the unnecessary details were removed from the voxel space.

Finally, as shown in Figure 17, the unevenly spaced Cartesian grid was automatically generated from the voxel shown in Figure 16. We used the same parameter settings as in Section 4.1 in the grid generation. The number of generated grid points was 629 in the width, 358 in the depth, and 102 in the height. The maximum and minimum grid widths were 0.1 and 0.025 m in all axes. The grid generation time was 13 min 46 sec, excluding user interaction and registration time.

From the comparison between Figure 9 and 16, and Figure 10 and 17, although small differences in the spatial occupancy classification results in the voxel space were overserved, there was no significant difference in the CFD grid structure between the simulated and real laser-scanned point clouds.

An airflow velocity analysis similar to that in Section 4.1 was performed with CFD simulation software using the unevenly spaced grid generated from the real-scanned points. Figure 18 showed the analysis results. The CFD simulation took 5 h 44 min to predict the phenomenon for 33 sec. A comparison of Figures 11 and 18 showed that there was no significant difference in the airflow simulation result between the simulated and real laser-scanned point clouds.



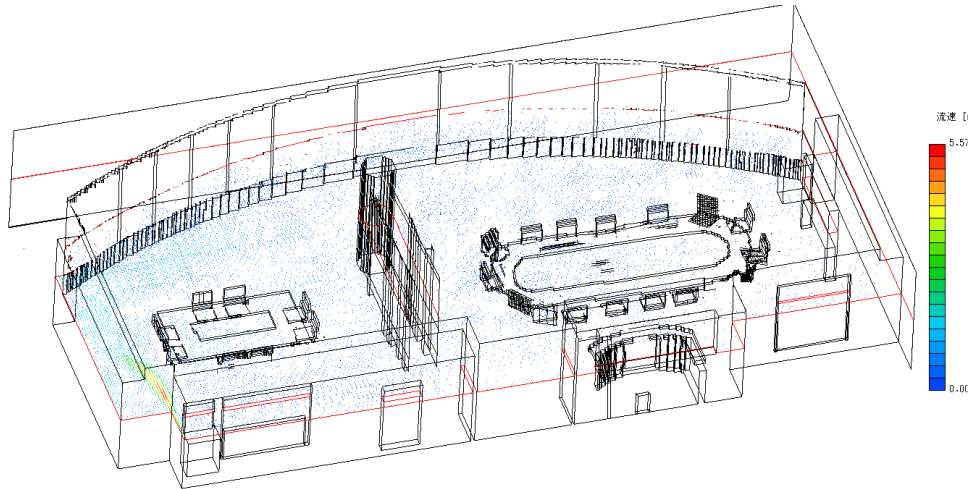


**Figure 18:** Airflow simulation result using the Cartesian grid of Figure 17 generated from the real laser-scanned point clouds of Figure 13.

Consequently, it was confirmed that the proposed method could semi-automatically generate the unevenly spaced Cartesian grids directly from laser-scanned point clouds of indoor spaces, and the grid could be effectively used in as-built CFD analysis.

## 5 CONCLUSIONS

We proposed a method to directly generate the unevenly spaced Cartesian grids from the laser-scanned point clouds of the existing indoor space for as-built CFD analysis. The method does not require any 3D CAD model in the grid generation. By using the proposed method, the CFD analysis could be conducted by using both the simulated and real scanned points. The comparison of the analysis between dense and evenly spaced grids also showed that our method sufficiently ensured the analysis accuracy using the unevenly spaced Cartesian grid with a smaller grid size obtained by our method. It is also confirmed that there is no significant difference in the CFD grid structure and the airflow simulation result between the simulated and real laser-scanned point clouds.

This study is an initial investigation to suggest a possible beneficial effect of the integration of 3D laser scanning with as-built CFD analysis. Therefore, the problems yet to be solved are listed below:

- The constraint on the allowable aspect ratio of grid width will be visible in the current grid generation algorithm.
- The special objects (heat source, louver and so on) to which the boundary conditions of the CFD analysis are added should be automatically detected in the point clouds. 3D object detection and instance segmentation techniques based on model-based recognition or machine learning could be used for detection.
- If the difference in materials among object surfaces can be recognized, it would lead to greater efficiency in the heat conduction condition assignments for the surfaces. Although the material discrimination ability by only using the laser-scanned point is unreliable so far, recent deep learning techniques might realize it.
- The robustness of grid generation against the measurement errors and occlusions of the laser scan should be investigated. Additionally, more case studies are needed to evaluate the accuracy and efficiency of the proposed method.

- The comparison of the CFD simulation results with the real world should be conducted experimentally.
- Moreover, in our current system, the user must still interactively assign the free or occupied label to the clusters of unknown voxels to solve the uncertainty of occupancy. This manual effort would be alleviated by introducing a computer-aided optimal scan planning technique of laser scanner placements. The scanner setup positions could be arranged before the actual measurement so that the unknown voxels could be minimized [8][30]. Since we have already developed such a system [33], we will approach the integration of the optimal scan-planning system with the grid generation system in the future.

Tetsuro Ishikawa, <https://orcid.org/0000-0001-9628-4658>

Satoshi Kanai, <https://orcid.org/0000-0003-3570-1782>

Hiroaki Date, <https://orcid.org/0000-0002-6189-2044>

## ACKNOWLEDGEMENT

The authors would like to express the deepest appreciation to Dr. Eisuke Wakisaka and Mr. Ken Fukada at R&D center in Shinryo Corporation who provided us the indoor space model and laser scanned points and their insightful comments and suggestions for CFD grid generation and analysis. The authors would also like to thank Enago ([www.enago.jp](http://www.enago.jp)) for the English language review.

## REFERENCES

- [1] Ahrens, J.P.; Geveci, B.; Law, C.C.: ParaView: An End-User Tool for Large-Data Visualization. The Visualization Handbook, Elsevier, 2005. ISBN: 9780123875822
- [2] Barazzetti, L.; Banfi, F.; Brumana, R.; Gusmeroli, G., Oreni, D., Previtali M.; Roncoroni, F.; Schiantarelli, G.: BIM from laser clouds and finite element analysis: combining structural analysis and geometric complexity, Int. Arch. Photogramm. Remote Sens. Spatial Inf. Sci., XL-5/W4, 2015, 345–350. <https://doi.org/10.5194/isprsarchives-XL-5-W4-345-2015>
- [3] Biljecki, F.; Stoter, J.; Ledoux, H.; Zlatanova, S.; Çöltekin, A.: Applications of 3D city models: state of the art review, ISPRS Int. J. Geo-Inf., 4(4), 2015, 2842–2889. <https://doi.org/10.3390/ijgi4042842>
- [4] Castellazzi, G.; D'Altri, A. M.; Bitelli, G.; Selvaggi, I.; Lambertini, A.: From laser scanning to finite element analysis of complex buildings by using a semi-automatic procedure, Sensors, 15(8), 2015, 18360–18380. <https://doi.org/10.3390/s150818360>
- [5] Castellazzi, G.; D'Altri, A.-M.; de Miranda, S.; Ubertini, F.: An innovative numerical modeling strategy for the structural analysis of historical monumental buildings, Engineering Structures, 132, 2017, 229–248. <https://doi.org/10.1016/j.engstruct.2016.11.032>
- [6] E. Recast: Directive 2010/31/EU of the European Parliament and of the Council of 19 May 2010 on the energy performance of buildings (recast), Off J Eur Union, 18, 2010, 2010.
- [7] Fouquier, A.; Robert, S.; Suard, F.; Stéphan, L.; Jay, A.: State of the art in building modelling and energy performances prediction: A review, Renewable and Sustainable Energy Reviews, 23, 2013, 272–288. <https://doi.org/10.1016/j.rser.2013.03.004>
- [8] Giorgini, M.; Marini, S.; Monica, R.; Aleotti, J.: Sensor-based optimization of terrestrial laser scanning measurement setup on GPU, IEEE Geoscience and Remote Sensing Letters, 16(9), 2019, 1452–1456. <https://doi.org/10.1109/LGRS.2019.2899681>
- [9] Gschwandtner M.; Kwitt R.; Uhl A.; Pree W.: BlenSor: Blender Sensor Simulation Toolbox, Lecture Notes in Computer Science, 6939, 2011. <https://www.blenzor.org/pages/publications.html>
- [10] Guarnieri, A.; Milan, N.; Vettore, A.: Monitoring of complex structure for structural control using terrestrial laser scanning (Tls) an photogrammetry, International Journal of Architectural Heritage, 7(1), 2013, 54–67. <https://doi.org/10.1080/15583058.2011.606595>

- [11] Hinks, T.; Carr, H.; Truong-Hong, L.; Laefer, D.-F.: Point cloud data conversion into solid models via point-based voxelization, *J. Surv. Eng.*, 139(2), 2013, 72-83. [https://doi.org/10.1061/\(ASCE\)SU.1943-5428.0000097](https://doi.org/10.1061/(ASCE)SU.1943-5428.0000097)
- [12] Hornung, A.; Wurm, K.-M.; Bennewitz, M.; Stachniss, C.; Burgard, W.: OctoMap: An efficient probabilistic 3D mapping framework based on Octrees, *Autonomous Robots*, 34(3), 2013, 189-206. <https://doi.org/10.1007/s10514-012-9321-0>
- [13] Hsieh, C.-M.; Aramaki, T.; Hanaki, K.: Managing heat rejected from air conditioning systems to save energy and improve the microclimates of residential buildings, *Computers, Environment and Urban Systems*, 35(5), 2011, 358-367. <https://doi.org/10.1016/j.compenvurbsys.2011.02.001>
- [14] InfiPoints: Modeling directly from laser scans to Autodesk Revit with InfiPoints: Improving 3D point cloud and BIM interoperability, <https://www.spar3d.com/sponsored/sponsored-software/modeling-directly-from-laser-scans-to-autodesk-revit-with-infipoints-improving-3d-point-cloud-and-bim-interoperability/>
- [15] Janßen, C.; Koliha, N.; Rung, T.: A fast and rigorously parallel surface voxelization technique for GPU-Accelerated CFD Simulations, *Communications in Computational Physics*, 17(5), 2015, 1246-1270. <https://doi.org/10.4208/cicp.2014.m414>
- [16] Janssen, W.D.; Blocken, B.; van Hooff, T.: Pedestrian wind comfort around buildings: Comparison of wind comfort criteria based on whole-flow field data for a complex case study, *Building and Environment*, 59, 2013, 547-562. <https://doi.org/10.1016/j.buildenv.2012.10.012>
- [17] Jung, J.; Hong, S.; Jeong, S.; Kim, S.; Cho, H.; Hong, S.; Heo, J.: Productive modeling for development of as-built BIM of existing indoor structures, *Automation in Construction*, 42, 2014, 68-77. <https://doi.org/10.1016/j.autcon.2014.02.021>
- [18] Lahur, P.; Hashimoto, A.; Murakami, K.: Automatic grid generation for dirty STL data using approximate concave feature, 50th AIAA Aerospace Sciences Meeting including the New Horizons Forum and Aerospace Exposition, 2012. <https://doi.org/10.2514/6.2012-154>
- [19] Lehtola, V.V.; Kaartinen, H.; Nüchter, A.; Kaijaluoto, R.; Kukko, A.; Litkey, P.; Honkavaara, E.; Rosnell, T.; Vaaja, M.T.; Virtanen, J.-P.; Kurkela, M.; El Issaoui, A.; Zhu, L.; Jaakkola, A.; Hyyppä, J.: Comparison of the selected state-of-the-art 3D indoor scanning and point cloud generation methods, *Remote Sens*, 9(8), 2017, 796. <https://doi.org/10.3390/rs9080796>
- [20] Liu, J.; Zhu, S.; Kim, M.-K.; Srebric, J.: A review of CFD analysis methods for personalized ventilation (PV) in indoor built environments, *Sustainability*, 11, 2019, 4166. <https://doi.org/10.3390/su11154166>
- [21] Lubowiecka, I.; Armesto, J.; Arias, P.; Lorenzo, H.: Historic bridge modelling using laser scanning, ground penetrating radar and finite element methods in the context of structural dynamics, *Engineering Structures*, 31(11), 2009, 2667-2676. <https://doi.org/10.1016/j.engstruct.2009.06.018>
- [22] Macher, H.; Landes, T.; Grussenmeyer, P.: From point clouds to building information models: 3D semi-automatic reconstruction of indoors of existing buildings, *Appl. Sci.*, 7(1), 2017, 1030. <https://doi.org/10.3390/app7101030>
- [23] Maragkogiannis, K.; Kolokotsa, D.; Maravelakis, E.; Konstantaras, A.: Combining terrestrial laser scanning and computational fluid dynamics for the study of the urban thermal environment, *Sustainable Cities and Society*, 13, 2014, 207-216. <https://doi.org/10.1016/j.scs.2013.12.002>
- [24] Ochmann, S.; Vock, R.; Klein, R.: Automatic reconstruction of fully volumetric 3D building models from oriented point clouds, *ISPRS Journal of Photogrammetry and Remote Sensing*, 151, 2019, 251-262. <https://doi.org/10.1016/j.isprsjprs.2019.03.017>
- [25] Pérez-Lombard, L.; Ortiz, J.; Pout, C.: A review on buildings energy consumption information, *Energy and Buildings*, 40(3), 2008, 394-398. <https://doi.org/10.1016/j.enbuild.2007.03.007>
- [26] Sanhudo, L.; Ramos, N.-M.M.; Martins, J.-P.; Almeida, R.-M.S.F.; Barreira, E.; Simões, M.-L.; Cardoso, V.: Building information modeling for energy retrofitting – A review, *Renewable and Sustainable Energy Reviews*, 89, 2018, 249-260. <https://doi.org/10.1016/j.rser.2018.03.064>

- [27] scSTREAM, <https://www.cradle-cfd.com/product/scstream.html>, Software Cradle.
- [28] Tan, G.; Glicksman, L.-R.: Application of integrating multi-zone model with CFD simulation to natural ventilation prediction, *Energy and Buildings*, 37(10), 2005, 1049-1057. <https://doi.org/10.1016/j.enbuild.2004.12.009>
- [29] Tang, P.; Huber, D.; Akinci, B.; Lipman, R.; Lytle, A.: Automatic reconstruction of as-built building information models from laser-scanned point clouds: A review of related techniques, *Automation in Construction*, 19(7), 2010, 829-843. <https://doi.org/10.1016/j.autcon.2010.06.007>
- [30] Tang, P.; Alaswad, F.-S.: Sensor modeling of laser scanners for automated scan planning on construction jobsites, *Proceedings of the 2012 Construction Research Congress*, 2012, 1021-1031. <https://doi.org/10.1061/9780784412329.103>
- [31] Toparlar, Y.; Blocken, B.; Maiheu, B.; van Heijst, G.J.F.: A review on the CFD analysis of urban microclimate, *Renewable and Sustainable Energy Reviews*, 80, 2017, 1613-1640. <https://doi.org/10.1016/j.rser.2017.05.248>
- [32] Tran, H.; Khoshelham, K.; Kealy, A.; Diaz-Vilarino, L.: Shape grammar approach to 3D modeling of indoor environments using point clouds. *Journal of Computing in Civil Engineering*, 33(1), 2019, 04018055. [https://doi.org/10.1061/\(ASCE\)CP.1943-5487.0000800](https://doi.org/10.1061/(ASCE)CP.1943-5487.0000800)
- [33] Wakisaka, E.; Kanai, S.; Date, H.: Model-based next-best-view planning of terrestrial laser scanner for HVAC facility renovation, *Computer-Aided Design and Applications*, 15(3), 2018, 353-366. <https://doi.org/10.1080/16864360.2017.1397886>
- [34] Xie, L.; Wang, R.: Automatic indoor building reconstruction from mobile laser scanning data, *Int. Arch. Photogramm. Remote Sens. Spatial Inf. Sci.*, XLII-2/W7, 2017, 417-422. <https://doi.org/10.5194/isprs-archives-XLII-2-W7-417-2017>